Modulation of the mechanism of apoptosis in cancer cell lines by treatment with silica-based nanostructured materials functionalized with different metallodrugs

Diana Díaz-García[a], Diana Cenariu[b], Yolanda Pérez[a], Paula Cruz[a], Isabel del Hierro[a], Sanjiv Prashar[a], Eva Fischer-Fodor[b,c,*] and Santiago Gómez-Ruiz[a,*]

[a] *Departamento de Biología y Geología, Física y Química Inorgánica, ESCET, Universidad Rey Juan Carlos, Calle Tulipán s/n, E-28933, Móstoles (Madrid), Spain*

[b] *Medfuture - Research Center for Advanced Medicine, The University of Medicine and Pharmacy "Iuliu Hatieganu", RO-400337, Cluj-Napoca, Romania.*

[c] *Tumour Biology Department, The Institute of Oncology "I.Chiricuta", RO-400015, Cluj-Napoca, Romania.*

† *Corresponding authors: S. Gómez-Ruiz, *e-mail address*: santiago.gomez@urjc.es and E. Fischer-Fodor, *e-mail address*: fischer.eva@iocn.ro

Electronic Supplementary Information (ESI) available: Supplementary material contains: Pore size distribution of SBA-PADOH and **M1**–**M3**, FT-IR spectra of SBA-PADOH and **M1**–**M3**, DR-UV spectra of SBA-PADOH and **M1**–**M3**, particle size distribution of SBA-PADOH and **M1**–**M3**, and some figures of additional biological studies. See DOI: 10.1039/x0xx00000x

Abstract

The mesoporous silica-based material SBA-15 (Santa Barbara Amorphous-15) has been modified with the aminodiol ligand 3-[bis(2-hydroxyethyl)amino]propyltriethoxysilane (PADOH) to give the corresponding material SBA-PADOH. Subsequent functionalization with a diorganotin(IV) compound, $SnPh_2Cl_2$ (**1**), and with two titanocene derivatives, $TiCp_2Cl_2$ ($[Ti(\eta^5\text{-}C_5H_5)_2Cl_2]$ (**2**)) and $TiCpCp^{PhNf}Cl_2$ ($[Ti(\eta^5\text{-}C_5H_5)(\eta^5\text{-}C_5H_4CHPhNf)Cl_2]$ (**3**) (Ph = C_6H_5; Nf = $C_{10}H_7$)), gave the materials SBA-PADO-$SnPh_2$ (**M1**), SBA-PADO-$TiCp_2$ (**M2**) and SBA-PADO-TiCpCp* (**M3**), respectively. SBA-PADOH and **M1**–**M3** have been characterized by various techniques such as FT-IR, XRD, XRF, solid-state NMR, nitrogen adsorption-desorption isotherms, electrochemical methods, SEM and TEM, observing that the functionalization has mainly taken place inside the pores of the corresponding porous system. In addition, mechanistic aspects of the apoptosis triggered by the synthesized materials have been studied *in vitro* in tumour cell lines derived from three distinct types of cancer in order to elucidate their growth inhibition and interference with the expression of tumour necrosis factor alfa (TNF-α) and the first apoptosis signal receptor (Fas or tumour necrosis factor receptor 6). It was observed that the antiproliferative and proapoptotic capacity of the materials depends on their functionalization with the different cytotoxic prodrugs (organotin or titanocene derivatives). The study shows that **M1**–**M3** influence the metabolic activity of the tumour cells and modulate the apoptotic pathways by different mechanisms, according to the active compound inside the material.

Keywords: SBA-15; titanocene; diorganotin; cytotoxicity; apoptosis; TNF-α; Fas receptor

Introduction

The use of metal-based drugs in cancer chemotherapy has greatly increased since the discovery and approval by the FDA of the use of cisplatin for the treatment of ovarian and testicular cancer in 1978.[1] Following on from the application of platinum-based compounds against different tumours, a wide variety of alternative drugs based on other metal complexes have been developed and studied in vitro and in preclinical and clinical trials.[2,3]

In this context, the literature is full of examples of synthesis, characterization and study of the cytotoxic properties of metal-based drugs as alternatives to platinum complexes.[2,4,5] In particular, titanium(IV) compounds have exhibited very interesting properties against a wide variety of cancer cell lines and have also been used in preclinical and clinical trials with promising results.[6,7,8,9,10] In addition, organotin(IV) compounds have also emerged as promising candidates because of their potent cytotoxicity[11,12] and their ability to overcome multidrug resistance (MDR) as some of them are not substrates of the Pgp-protein. This protein pumps out of the cell most of the administered anticancer drugs, decreasing their therapeutic efficacy.[13] Therefore, metal complexes based on titanium and tin have attracted the interest of the scientific community and are currently in continuous development.

However, the high number of side effects associated with the use of platinum and other metal complexes in chemotherapy,[14] together with low water solubility, speciation in physiological medium and acquisition of resistance by some of the treated cells of the tumours, has refocused the interest of researchers. Thus, different alternatives for the administration of metallodrugs are being studied, with the principle aims of avoiding or diminishing the decomposition processes during the transport to cells, addressing their low water solubility and promoting an effective protection of the metal-containing active species.[15,16]

Thus, the encapsulation or incorporation of metal-based therapeutic systems in different scaffolds, usually porous and nanosized systems, helps enhance the cytotoxic properties of the studied metallodrugs and thus improving their effectivity *in vitro* and *in vivo*.[15] The systems used as encapsulators or carrier vectors for the administration of metal-based drugs are varied and comprise materials based on different scaffolds such as organic polymeric nanoparticles, proteins, metal and metal oxide nanosystems, carbon nanostructures, ceramic materials and polyoxometalates.[15,17,18,19,20,21,22,23,24, 25,26]

Our group has focused its attention on the use of nanostructured porous silica-based materials as encapsulators of metal-based drugs based on titanium[15,16,27,28,29,30,31,32,33] and tin[34,35] which have shown interesting properties in vitro and in vivo against a wide variety of cancers. Indeed, the elucidation of the mechanism of action of these materials is interesting from a medicinal point of view as they usually do not act as classical drug-delivery systems. They have a high cytotoxic action without apparently the need of releasing the loaded anticancer metallodrug thus considering their action to be due to the entire nanoparticulated system. This has been observed by our group and opens up the possibility of testing several anticancer metallodrugs which have been disregarded because of their lack of solubility or low stability in physiological medium. In addition, these metallodrug-functionalized nanostructured silica-based materials have shown the enhancement of the metal uptake by the cancer cells in cytotoxic experiments in vitro, following a completely different mechanism of cell death compared to that of the free metallodrugs.

All these experiments carried out by our group have led us to gain insights on cellular cytotoxic mechanism of action promoted by these materials in cancer cells. Thus, we have

observed that the metallodrug-functionalized materials induce the programmed cell death by impairing the damaged DNA repair mechanism and upregulating intrinsic and extrinsic apoptosis signalling pathways.[15,36] In addition, we have recently observed that certain titanocene-functionalized nanostructured silica materials are able to induce cell growth inhibition by interfering with the metabolic activity of the cell and through TNFR1 modulation.[32]

In the present study we describe our efforts in elucidating mechanistic aspects of the apoptosis induction and the differences in the biological action of promoted by organotin- and titanocene-functionalized SBA-PADOH materials *in vitro* in tumour cell lines derived from three distinct types of cancer. In this context, we have considered TNF-α due to its role as an important biological marker in inflammatory and apoptotic processes. This arises from its binding with TNFR1 which in the way it takes place can be indicative of the different mechanisms leading to cancer cell death.[37,38,39,40] We have examined the growth inhibition and the capacity to interfere with the expression of tumour necrosis factor alfa (TNF-α) and the first apoptosis signal receptor (Fas or tumour necrosis factor receptor 6), both being important players in the extrinsic apoptotic pathways.

Experimental Section

General remarks on the synthesis and characterization of the materials

All reactions were performed using standard Schlenk tube techniques in an atmosphere of dry nitrogen. Solvents and triethylamine were distilled from the appropriate drying agents and degassed before use. The reagents used in the preparation of the corresponding metallodrug-functionalized nanostructured materials such as $[TiCl_4(THF)_2]$, $[Ti(\eta^5\text{-}C_5H_5)_2Cl_2]$, $[Ti(\eta^5\text{-}C_5H_5)Cl_3]$, $SnPh_2Cl_2$, TEOS, Pluronic 123 and 3-[bis(2-hydroxyethyl)amino]propyltriethoxysilane (PADOH) and hexamethyldisilazane (HMDS) were purchased from Sigma Aldrich and used directly without further purification. Pyrrolidine, LiPh (1.8 M in dibutylether) and $C_{10}H_7CHO$ for the synthesis of (C_5H_4)=CHNf, Li{C_5H_4(CHPhNf)} and $[Ti(\eta^5\text{-}C_5H_5)(\eta^5\text{-}C_5H_4CHPhNf)Cl_2]$ (**3**) were purchased from Aldrich and used directly. Preparation of **3** was carried out following the same synthetic method described by us.[41]

^{13}C-CP MAS spectra, were recorded on a Varian-Infinity Plus Spectrometer at 400 MHz operating at 100.52 MHz proton frequency (4 μs 90° pulse, 4000 transients, spinning speed of 6 MHz, contact time 3 ms, pulse delay 1.5 s). X-ray diffraction (XRD) pattern of the silicas were obtained on a Philips Diffractometer model PW3040/00 X'Pert MPD/MRD at 45 kV and 40 mA, using a wavelength Cu Kα (λ = 1.5418 Å). Ti and Sn wt % determination by X-ray fluorescence were carried out with an X-ray fluorescence spectrophotometer Phillips MagiX with a X-ray source of 1 kW and a Rh anode using a helium atmosphere. The quantification method is able to analyze from 0.0001% to 100% titanium and sulphur. N_2 gas adsorption-desorption isotherms were performed using a Micromeritics ASAP 2020 analyzer. Scanning electron micrographs and morphological analysis were carried out on a XL30 ESEM Philips with an energy dispersive spectrometry system (EDS). The samples were treated with a sputtering method with the following parameters: Sputter time 100 s, Sputter current 30 mA, film thickness 20 nm using a Sputter coater BAL-TEC SCD 005. Conventional transmission electron microscopy (TEM) was carried out on a TECNAI 20 Philips, operating at 200 kV.

Synthesis of SBA-15

The synthesis of SBA-15 was carried out following the experimental procedure reported by Zhao *et al.*[42] An aqueous solution of TEOS 98% (102 g, 0.480 mol) was prepared and added dropwise to a stirring solution (1000 rpm) containing the Pluronic 123 surfactant (48.4 g) in 360 mL of Milli-Q water and 1342 mL of HCl 2 M at 35 °C. The reaction was stirred (1000 rpm) at 35 °C for 20 h more to form a white solid. Stirring was then stopped and the temperature was increased to 80 °C and maintained for 24 h in order to complete the ageing process. The suspension was then filtered under vacuum and the resulting white solid washed abundantly with Milli-Q water to remove impurities and the remaining surfactant. After washing, a drying process (at 100 °C during 18 h) and a final calcination process (during 24 h at 500 ºC) in a muffle oven were carried out. After the calcination process 26.88 g of a fine white powder of SBA-15 were obtained and used for the characterization tests and subsequent functionalization reactions with PADOH.

Functionalization of SBA-15-PADOH in the presence of hexamethyldisilazane as capping agent

SBA-15 was treated with the aminodiol ligand 3-[bis(2-hydroxyethyl)amino]-propyltriethoxysilane in the presence of hexamethyldisilazane (to reduce the number of free silanol groups in the surface of the material). The synthesis was carried out using the procedure recently reported by our group.[43] 10 g of SBA-15 mesoporous silica was suspended in 300 mL of dry toluene and hexamethyldisilazane (HMDS) (8.40 mL, 40 mmol). 3-[bis(2-hydroxyethyl)-amino]propyltriethoxysilane in ethanol (20 mL, 40 mmol) was then simultaneously added dropwise. The reaction mixture was then stirred for 48 h at 110 °C and the resulting solid isolated by filtration and washed with toluene (2 × 100 mL) and hexane (2 × 100 mL). The final material was dried under vacuum at room temperature and stored under nitrogen.

Synthesis of SBA-PADO-$SnPh_2$ (M1)

A solution of $SnPh_2Cl_2$, (0.58 g, to obtain a theoretical level of 15% Sn/SiO_2) in toluene (60 mL) was added to SBA-PADOH (1.50 g). Subsequently, 4.0 mL of triethylamine was added and the mixture was stirred overnight at 120 °C for 48 hours. The slurry was then filtered through fritted discs and the solid residue washed with toluene (2 × 40 mL), and a 1:1 mixture of water:ethanol (2 × 40 mL). The resultant solid was dried at 70 °C for 16 hours and under vacuum at room temperature for 4 additional hours to give a white free flowing powder. XRD (2Θ, º) 0.97 (100), 1.98 (110); BET surface area 286 m^2/g; pore size 3.52 nm; ^{13}C CP MAS NMR (ppm): 2 (O-$SiMe_3$), 9 and 21 (-CH_2-), 52 and 61 (N-CH_2-CH_2-O), 130 and 142 (Ph); FRX: 12.5 % wt. Sn and 1.0 % wt. Cl.

Synthesis of SBA-PADO-$TiCp_2$ (M2)

The synthesis of material **M2** was carried out in identical manner to that of **M1**. [Ti(η^5-$C_5H_5)_2Cl_2$] (**2**) (0.36 g, to obtain a theoretical level of 5% Ti/SiO_2), SBA-PADOH (1.50 g) and triethylamine (4.0 mL). XRD (2Θ, º) 1.01 (100), 1.97 (110); BET surface area 347 m^2/g; pore size 3.32 nm; ^{13}C CP MAS NMR (ppm): 2 (O-$SiMe_3$), 9, 20, 31 and 43 (-CH_2-), 48, 52 and 62 (N-CH_2-CH_2-O), 117 (Cp); FRX: 3.2 % wt. Ti and 2.2 % wt. Cl.

Synthesis of SBA-PADO-TiCpCp* (M3)

The synthesis of material **M3** was carried out in identical manner to that of **M1**. [Ti(η^5-C_5H_5)(η^5-C_5H_4CHPhNf)Cl_2] (**3**) (0.62 g, to obtain a theoretical level of 5% Ti/SiO_2), SBA-PADOH (1.50 g) and triethylamine (4.0 mL). XRD (2Θ, º) 1.04 (100), 1.98 (110); BET surface area 275 m^2/g; pore size 3.62 nm; ^{13}C CP MAS NMR (ppm): 1 (O-$SiMe_3$), 10 and 23 (-CH_2-), 51 and 60 (N-CH_2-CH_2-O), 70 (CH attached to Cp), 117 and 128 (Cp, Nf, Ph); FRX: 2.0 % wt. Ti and 0.8 % wt. Cl.

Metal ions-release studies

Tin and titanium release of the materials in biological conditions was carried out in a body simulated fluid (pH 7.4 buffer) prepared according to reported procedures.[44] In duplicate, 10 mL of simulated body fluid was added to 15 mg of the studied materials. These suspensions were incubated at 37 ºC in a water bath for 1, 6, 24, 48 and 96 h. Afterwards, the suspension was filtered through a nylon filter (0.2 µm). The solution was then analysed by ICP-AES, using a Varian Vista AX Pro Varian 720-ES instrument.

Materials and methods for in vitro cytotoxicity and apoptosis tests

The *in vitro* testing was performed on immortal tumour cell lines: human DLD-1 colon carcinoma, A2780 ovarian carcinoma and A431 epidermoid carcinoma (cell lines acquired from European Collection of Cell Cultures (ECACC). DLD-1 and A2780 cells were cultivated in RPMI-1640 cell culture media, supplemented with 10% foetal calf serum; the A431 cells in DMEM media with 4500 mg/L glucose, sodium pyruvate and 10% foetal calf serum. All media and supplements were purchased from Sigma Aldrich Company, St. Louis, USA.

For the viability testing, the cells were cultivated on 96-well plates, at a concentration of 1.5×10^4 cells seeded with 200 µL media in each well. For the single-cell membrane markers and for the soluble proteins evaluation testing, the cells were seeded on 6-well plates, at a density of 2.5×10^5 cells in 3 mL on each well. In every experiment, after a 24-hours period, while cells adhered to the plates and the proliferation process begun, the PADOH derivatives were added. The cells were evaluated after 24 hour treatment in each measurement. Untreated cells were used as reference values, and cell culture media as blank.

SBA-PADOH, SBA-PADO-$SnPh_2$ (**M1**), SBA-PADO-$TiCp_2$ (**M2**) and SBA-PADO-TiCpCp^{PhNf} (**M3**) were dispersed in dimethyl sulfoxide (DMSO, from Merck KGaA, Darmstadt, Germany) at a concentration of 100 mg/mL. These stock suspensions were diluted in phosphate buffered saline solution (PBS, from Sigma Aldrich), to obtain 8 serial dilutions from 10 µg/mL to 5000 µg/mL. The active precursors included in materials were also tested; they were diluted in DMSO, then serial dilutions were made in PBS, to obtain the analogous concentration ranges of the free precursors: 1.24 to 610 µg/mL $SnPh_2Cl_2$; 0.32 to 160 µg/mL $TiCp_2Cl_2$ and 0.20 to 100 µg/mL TiCpCp$^{PhNf}Cl_2$. An additional concentration was included for precursors: 10% of the lowest analogue concentration, considering their capacity to release around 10% of active compound. For the viability testing, the dispersed materials replaced a proportion of 1/20 of the cell culture media. To establish the half maximal effective concentrations (EC_{50}), we evaluated the mitochondrial activity with the colorimetric MTT method, as described earlier.[45]

The same treatment and concentrations were used for the evaluation of metabolic activity; the cells capacity to convert resazurin (Alamar Blue reagent from Invitrogen, Thermo Fisher Scientific, Waltham, USA) into resorufin was performed by fluorimetric quantification.[46]

To evaluate the proportion of apoptotic cells within the tumour cell population, 6-well plates were used, where 2×10^5 cells were in 2.5 mL media in each well. The cells were treated with SBA-PADOH, $SnPh_2Cl_2$, $TiCp_2Cl_2$, $TiCpCp^{PhNf}Cl_2$, SBA-PADO-$SnPh_2$ (**M1**), SBA-PADO-$TiCp_2$ (**M2**) and SBA-PADO-TiCpCp* (**M3**) for 24 hours; the sub-lethal final concentration of 200 µg/mL in the cell culture media was used for each material. Each sample was prepared in duplicate. The cells were harvested from the plate, including the detached, floating cells from the cell culture media. For apoptosis evaluation, the Alexa Fluor 488 labelled Anexin V, and the propidium iodide (PI) viability dye were used (Apoptosis kit from Invitrogen, Applied Biosystems Carlsbad, CA, USA). The cells were washed, resuspended in the binding buffer provided by the manufacturer, then incubated with the dyes and subjected to flow cytometry analysis according to the manufacturers protocol. Samples were analysed by flow cytometry, with a FACS Canto II Flow cytometer, (BD Biosciences, San Jose, CA, USA). Alexa Flour 488 dye (green) was detected using the 530/30 filter and PI (red) with the 575/26 filter. The total number of apoptotic cells, coloured in green, can be examined as two distinct subsets: the early apoptotic cells, labelled only with Annexin V, and the late apoptotic cells, having double green and red colouration, while the dead cells appear with intracytoplasmic red fluorescence.

To perform the Elisa testing, the cells were cultivated on 6-well plates. 2×10^5 cells were seeded in 2.5 mL media and subsequently the cells attached and the proliferation begun. The cells were treated with 200 µg/mL SBA-PADOH, the active metal complexes and the functionalized materials **M1**-**M3**. Considering the metal content of **M1**, **M2** and **M3**, the concentration of precursors were chosen accordingly: 24.8 µg/mL $SnPh_2Cl_2$; 6.4 µg/mL $TiCp_2Cl_2$and 4 µg/mL $TiCpCp^{PhNf}Cl_2$, respectively. Subsequently, the cell culture supernatants were harvested from the plates and their protein content was measured with the Bradford method. The samples were aliquoted and cryoconserved at -80 ºC. The soluble Fas and FasLigand sandwich Elisa kits were purchased from R&D Systems (Minneapolis, USA). Before the testing, the samples were thawed, centrifuged, and diluted with the calibrator diluent provided by the kit, to obtain normalized protein concentrations: 1.8 µg/mL for DLD-1 cells, 1.5 µg/mL for A2780 cells and 1.7 µg/mL for A431 cells. The quantitative measurement of the soluble Fas and FasL levels was made on antibody-coated 96-well plates, provided by the manufacturer. In each well 100 µL of assay diluent was added, then 50 µL of samples, a series of 8 standard protein solutions and blank were pipetted in the wells, each of them in duplicates. After 2 hours of incubation and four automated wash cycles, conjugate antibody was added to each well, followed by 2 h incubation. The plates were washed, substrate solution was pipetted in the wells and after 30 minutes, the stopping solution was added and the plates were subjected to colorimetric measurement at 450/540 nm. The TNF-α human Elisa kit was from Hycult Biotech (Uden, The Netherlands). To assess the TNF-α level in the samples, they were diluted with sample diluents provided by the kit, to obtain the same protein levels as described above. 100 µL of standard proteins or samples were dispensed on a stripwell antibody-coated plate, in duplicates, and they were incubated at room temperature for 1 hour. After repeated washing procedures, 100 µL tracer antibody was added to each well, and the samples were incubated another hour at room temperature. The plate was washed and 100 µL of streptavidin-peroxidase solution was added and finally TMB substrate and stopping solution. The plate was subjected to colorimetric measurements at 450/540 nm and quantitative data were obtained after absorbance data processing with the equipment's software.

The cells were cultivated in Steri-Cycle i160 CO_2 Incubator (from Thermo Scientific, Cleveland, USA) at 37 °C and 5% CO_2 concentration and the experiments were performed in Class II BSC laminar hoods (acquired from Esco, Changi, Singapore). Also used were: MPW-352-R centrifuge with swing-out rotor (from MPW Med Instruments, Warsaw, Poland), orbital shaker-incubator ES-20 (from Biosan, Riga, Latvia), Biobase MW9623 Micro plate washer (from Biobase, Shandong, China), ULF ultra-freezer 480W PRO2 (from EVERmed, Motteggiana, Italy). The colorimetric and fluorescence measurements were performed with the Spark10M microplate reader and Magellan software (from Tecan GmbH, Grodig, Austria). The data has been processed with the GraphPad Prism 5 software (from GraphPad Software, La Jolla, USA).

Results and Discussion

Synthesis and characterization of metallodrug-functionalized SBA-15 materials

SBA-15 was functionalized with the aminodiol ligand 3-[bis(2-hydroxyethyl)amino]propyl-triethoxysilane (PADOH) to give SBA-PADOH (Scheme 1). This material was obtained by a simple grafting reaction of PADOH and SBA-15 in the presence of excess hexamethyldisilazane, in order to reduce to a minimum the number of free silanol groups in the final material.

Subsequently, SBA-PADOH was reacted with three different metal complexes, namely the tin derivative $SnPh_2Cl_2$ (**1**)) and two titanocene compounds $TiCp_2Cl_2$ ([Ti(η^5-C_5H_5)$_2$Cl$_2$] (**2**)) and $TiCpCp^{PhNf}Cl_2$ ([Ti(η^5-C_5H_5)(η^5-C_5H_4CHPhNf)Cl$_2$] (**3**) (Ph = C_6H_5; Nf = $C_{10}H_7$)), the latter is functionalized with small aromatic rings. These metal complexes have previously demonstrated good cytotoxic and DNA-binding properties.[41] Protonolysis reactions of SBA-PADOH were carried out in the presence of an organic base such as triethylamine to promote the formation of the supported tin(IV) or titanocene(IV) alkoxide SBA-15-based materials SBA-PADO-$SnPh_2$ (**M1**), SBA-PADO-$TiCp_2$ (**M2**) and SBA-PADO-TiCpCp* (**M3**), respectively (Scheme 1)

Materials SBA-15, SBA-PADOH and **M1**-**M3** have been characterized by different techniques. The XRD diffractograms show the typical signals associated with the hexagonally ordered silica SBA-15, consisting of a very intense diffraction peak at ca. 0.9° corresponding to the (100) Miller plane and a second peak of much lower intensity at around 1.8° which is assigned to the (110) Miller plane (Figure 1). The position of the diffraction peaks did not change after functionalization of SBA-15 with the PADOH ligand, however, the intensity of the peaks in SBA-PADOH was much lower compared to that of the unmodified SBA-15. Furthermore, for the tin and titanium-functionalized materials **M1**–**M3**, the intensity of the peaks decreased compared with those of SBA-PADOH. These results confirm the functionalization of the SBA-15 inside the pores as the decrease of the can be attributed to the partial blockage of the dispersion points (pores) associated with the mesoscopic order of the SBA-15 structure. In addition, the observation of the diffraction peaks in the same position after functionalization with both PADOH and the metallodrugs suggest that the structural order of the synthesized material is maintained. Furthermore, in all cases, the diffractogram can be indexed as a hexagonal lattice with *d*-spacing values of between 82-95 Å (Table 1).

The metallodrug-functionalized materials **M1**–**M3** were also characterized by XRF in order to determine the metal content and thus the degree of functionalization (Table 2). The tin-functionalized material **M1** showed a 12.4% wt. of Sn with only 1.0% wt. of Cl, to give a Sn:Cl molar ratio of ca. 3.8:1, indicating that most of the tin-supported complex is in the form of a

dialkoxide derivative (Figure 2, species B of SBA-PADO-$SnPh_2$). The quantity of titanium in materials **M2** and **M3** was 3.2 and 2.0% wt., respectively. In addition, the amount of Cl in **M2** of ca. 2.2% wt. (to give a Ti:Cl molar ratio of 1.1:1) suggests that the major species is that in which only one Ti-Cl bond of the titanocene complex [Ti(η^5-C_5H_5)$_2$$Cl_2$] (**2**) has reacted with the PADOH ligand forming the fragment "Cp_2TiCl{$(OCH_2CH_2)(HOH_2CH_2CH_2)NCH_2CH_2CH_2Si(OEt)_2$}O-SBA-15" which has an Ti-Cl bond still intact (Figure 2, species A of SBA-PADO-$TiCp_2$). On the contrary, the amount of Cl in **M3** of 0.8% wt. suggests that both of the Ti-Cl bonds of the complex [Ti(η^5-C_5H_5)(η^5-$C_5H_4CHPhNf$)Cl_2] (**3**) have reacted with the PADOH ligand to give, as a major species "Cp*CpTi{$(OCH_2CH_2)_2NCH_2CH_2CH_2Si(OEt)_2$}O-SBA-15" (Figure 2, species B of SBA-PADO-TiCpCp*).

All the studied materials SBA-15, SBA-PADOH and **M1**–**M3** were characterized by nitrogen adsorption / desorption isotherms. The results show that all the synthesized materials give type IV isotherms (according to the IUPAC classification).[47,48] In addition, in all cases an H2b hysteresis loop is formed which can be correlated with a typical mesoporous material (Figure 3).[47,48] Table 3 summarizes all the obtained data. The sorption study showed that the BET surface area (S_{BET}) of the unmodified SBA-15 was of 931 m^2/g. However, after grafting of PADOH ligand the BET surface area decreased to 306 m^2/g in SBA-PADOH. In addition, the subsequent reaction with either the tin compound or the titanocene derivatives generally led to a slight decrease of the surface area (Table 3). The effect of the capillary condensation of nitrogen within the uniform mesoporous structure was also observed in all the studied systems at relative pressures (P/P_0) of ca. 0.4. However, the inflection position changed to lower relative pressures due to the effect of the functionalization with the different fragments.

Regarding the pore diameter of the studied materials, a decrease from ca. 5.4 nm of unmodified SBA-15 to ca. 3.3-3.6 nm for SBA-PADOH, **M1**–**M3** was observed in the BJH average pore diameter (Table 3, for pore size distribution see Figure S1-S4 of Supplementary Material). The pore volume also decreases after functionalization with PADOH or the metallodrugs. Therefore, the functionalization of the porous system based can be envisaged to take place inside the pores of the SBA-15 particles.

SBA-PADOH and the materials **M1**–**M3** were also characterized by ^{13}C CP MAS spectroscopy. The ^{13}C CP MAS spectrum of SBA-PADOH (Figure 4a) showed various signals between 0 and 70 ppm which were assigned to the different carbon atoms of the PADOH ligand and the $SiMe_3$ groups arising from the capping reaction with hexamethyldisilazane, specifically, a high intensity signal at ca. 0 ppm assigned to the carbon atoms of the $OSiMe_3$ and three signals between 3 and 20 ppm corresponding to the three carbon atoms of the methylene groups of PADOH ligand (Si-CH_2-CH_2-CH_2-N). Furthermore, between 50 and 60 ppm, two additional signals assigned to the carbon atoms of the methylene groups directly bound to alcohol groups (-N-CH_2-CH_2-OH) were observed.

M1 was also characterized by ^{13}C CP MAS spectroscopy (Figure 4b) observing, between 0 and 70 ppm, the signals described previously for SBA-PADOH with a slight modification in the chemical shifts and intensity, and various broad signals, between 120 and 140 ppm, which were assigned to the carbon atoms of the phenyl rings of the $SnPh_2$ moiety.

The ^{13}C CP MAS spectra of **M2** and **M3** also show the signals associated with the incorporation of the PADOH ligand and the $SiMe_3$ groups coming from the capping reaction with hexamethyldisilazane and additional signals in the aromatic region arising from the cyclopentadienyl ligands of the supported titanocene complexes. Thus, the spectrum of **M2**

shows a very broad signal at ca. 115 ppm corresponding to the carbon atoms of the C_5H_5 ligand (Figure 4c), while **M3** shows three broad signals between 110 and 130 which were assigned to the carbon atoms of the cyclopentadienyl ring and the phenyl and naphthyl fragments and a signal at ca. 80 ppm corresponding to the carbon atom directly bound to the substituted Cp ring (Figure 4d). Thus, the ^{13}C CP MAS spectra, confirm the incorporation of the PADOH ligand and the metallodrugs in the SBA-15 material. This functionalization was also corroborated by FT-IR spectroscopy (see Figures S5-S11 of Supplementary Material). Additionally, the materials were also characterized by DR-UV spectroscopy which shows the band corresponding to the Cp ligands of **M2** and **M3** (Figure S12 of Supplementary Material).

Finally, all the synthesized materials were characterized by SEM and TEM microscopy (Figure 5). The pictures taken by the microscopes showed no significant differences between the different functionalized SBA-15 materials. These systems can be identified as nanostructured rods of ca. 545-605 nm long and ca. 330-410 nm width with narrow size distributions as observed in Figures S13-S16 and Table S1 of Supplementary Material. Furthermore, the TEM micrographs showed a highly hexagonally ordered arrangement of the pores (Figure 5h) corresponding to SBA-15 materials. In addition, the images show the parallel distribution of the channels along the particles.

Electrochemical studies of metallodrug-functionalized SBA-15 materials

In this section, differential pulse voltammetry (DPV) measurements have been performed to test the electroactivity of the tin and titanium-functionalized SBA-15 materials **M1**–**M3**. The experiments have been carried out at room temperature, using a three-electrode-single compartment electrochemical cell. A modified carbon paste with **M1**–**M3** materials has been used as working electrode, a Ag/AgCl/KCl (3 M) as reference electrode and a platinum rod as counter electrode.

Differential pulse voltammograms of the materials synthesized have been studied. The voltammetric response recorded signals due to the metallic species tethered to the silica surface. Figure 6 shows the DPV recorded for **M1** immediately after immersion of the graphite/silica working electrode into the aqueous electrolyte solution and shows one cathodic peak at -1.00 V attributed to the couple Sn(IV)/Sn(II). Similarly, titanium tethered complexes **M2** and **M3** gave one reduction peak at -1.07 V and -1.10 V, respectively which can be assigned to the reduction process Ti(IV)/Ti(III) of penta- or tetra- coordinated titanium centres. Previous studies of our group with a titanium amine bis(alkoxy) complex immobilized in SBA-15 showed that this complex, possibly hexacoordinated after water incorporation to the metal coordination sphere, renders in aqueous solution a reduction peak at -1.46 V.[49] Therefore, our current results show that **M2** and **M3** which contain cyclopentadienyl ligands are less difficult to reduce than the previously reported titanium amine bis(alkoxy) complex supported on SBA-15. In addition, previous results from our group showed than the tethered complex a system, based on $Ti(OR)_2$-amine-bis(phenolate) supported onto SBA-15 and which presents an octahedral coordination environment in aqueous medium, showed a potential peak at -1.03 V. This result can be explained assuming a higher coordination environment for titanium in the $Ti(OR)_2$-amine-bis(phenolate)-based system due to the presence of electron-withdrawing aryloxo ligands, which increase the reduction potential value in comparison to **M2** and **M3** (which contain more electron donating fragments, namely the cyclopentadienyl ligands).[50] Finally, comparing **M2** and

M3, the introduction of a substituent on one of the cyclopentadienyl rings makes **M3** less sensitive to reduction slightly shifting its cathodic potential to more negative values (Figure 6).

Study of the release of metallodrug-functionalized SBA-15 materials in physiological medium

Release of tin- and titanium-containing species was studied in simulated body fluid (pH = 7.4) at 37 ºC for 1, 6, 24, 48 and 96 h. After separation of the material of the solution by filtration, the solution was studied by ICP (Table 4, Figures S17 and S18). The results show that, in the case of the Sn-containing material (**M1**) a low release (ca. 10% of the loaded tin) of tin-containing species occurred. The release is higher at longer times but it seems that reaches the maximum after only 24 hours. This is in agreement with our previous results in the field which have also shown a low release of tin-soluble species in simulated body fluid.[34,35] The release of the supported organotin complex may probably be due to the slow hydrolysis of the Sn-O bond which partially releases tin-containing soluble fragments which remain in solution.

On the other hand, the analysis of the physiological solutions obtained after release studies of titanium-containing materials (**M2** and **M3**) showed almost no titanium with quantities of titanium slightly above the detection limit of the ICP measurements. The released titanium quantities were of ca. 0.2 ppm, less than a 1% of the loaded titanium in **M2** or **M3**, see Table 4 and Figures S19 and S20 of supplementary material). The very low release of titanium in the physiological medium (less than 1% of the loaded Ti in the materials) may be due to a slow hydrolysis of the Ti-O bonds of the supported complexes which may give, in part, insoluble titanium dioxide which is filtered off before the ICP analysis of the solution. In addition, and more likely according to previous results of our research group, one cannot rule out the possibility of an insignificant release of titanium soluble species because of the relatively high stability of Ti-O-X bonds (X = Si or C) in physiological medium (pH 7.4).[27-33]

In both cases, as the quantity of released compound seems to be very small, the biological activity of the functionalized materials **M1**–**M3** is most likely due to a combination of the particle action (the most influential agent) and a very low amount of metal-containing soluble fragments released to the medium.

Biological Studies. Cytotoxic activity of metallodrug-functionalized materials

Following the MTT viability testing on treated human tumour cells *in vitro*, the materials half maximal effective concentrations were quantified through the EC_{50} values, derived from the nonlinear dose-response curves (Table 5). In all cell lines, human DLD-1 colon carcinoma, A2780 ovarian carcinoma and A431 epidermoid carcinoma, SBA-PADOH exhibited a modest cytotoxicity and showed the highest EC_{50} values. However, all the metallodrug-functionalized materials **M1**–**M3** showed a much higher cytotoxic activity. Notably, material **M3** functionalized with the substituted titanocene complex $[Ti(\eta^5\text{-}C_5H_5)(\eta^5\text{-}C_5H_4CHPhNf)Cl_2]$ (**3**) showed the lowest of the studied EC_{50} values in all cell lines with values from ca. 167 to 335 μg/mL (Table 5). In addition, the results obtained for both the tin or titanium-functionalized materials **M1**–**M3** showed that the most resistant cell line was A431, while the highly proliferative colon carcinoma cells DLD-1 were the most susceptible to the treatments with the studied materials. The toxicity of the active compounds $SnPh_2Cl_2$, $TiCp_2Cl_2$ and $TiCpCp^{PhNf}Cl_2$ was calculated and compared with those of the functionalized materials **M1**–**M3**. Alone, $TiCp_2Cl_2$ and $TiCpCp^{PhNf}Cl_2$ exhibited

considerably lower growth inhibition than the functionalized **M2** and **M3** materials, therefore, their incorporation into the material seem to be very important for the enhancement of the cytotoxic properties of the metallodrugs. In contrast, the cytotoxicity of the $SnPh_2Cl_2$ compound alone is comparable, if not somewhat lower than that of the material **M1** (Table 5).

Biological Studies. Influence of metallodrug-functionalized materials on tumour cells mitochondrial metabolic activity

The tumour cells treated *in vitro* with the studied materials **M1**–**M3** suffered a loss of the intracytoplasmic reducing potential which is an indicator of their metabolic activity. The measurements were based on the transformation inside the living cells of the resazurin dye into its fluorescent resorufin form. The negative slope derived from the linear regression of emitted fluorescence indicates that the metabolic activity was reduced in all cell lines, proportional with the steepness of the line (Figure 7).

All materials were able to decrease the metabolic activity of the cancer cells (Figure 7). However, there were significant differences between the SBA-PADOH material and the metallodrug-functionalized systems **M1**–**M3** with the latter showing a much stronger decrease of the metabolic activity. In all cell lines, there was a significant correlation between the fluorescence reduction, and the EC_{50} values (non-parametric Spearman correlation, p value 0.033 in DLD-1 cells; p value 0.042 in A2780 and p value 0.003 in A431 cells).

The active precursors $TiCp_2Cl_2$ and $TiCpCp^{PhNf}Cl_2$ influence on the metabolic rate was less important as that of the functionalized materials **M2** and **M3** (Figures S21-S23 of supplementary material). The metabolic rate reduction in carcinoma cells treated with free $SnPh_2Cl_2$ (without incorporation into the SBA-15 material, **M1**) was noteworthy only for $SnPh_2Cl_2$, but much lower compared with that of its functionalized counterpart **M1**.

Biological Studies. Apoptosis induction promoted by metallodrug-functionalized materials

The 24-hours exposure of the tumour cells to sub-cytotoxic concentrations of the SBA-PADOH material and the metallodrug-functionalized systems, **M1**–**M3**, provided four distinct cellular subsets, evidenced by fluorescent colourations; the viable unaffected cells were unstained, the apoptotic cells labelled with green Alexa fluor 488-Annexin V conjugate, dead cells had red PI colouration on their nucleus and late apoptotic cells had double colouration (Figure 8). The number of viable cells was inversely correlated with the cytotoxicity of the materials. Thus, in the populations exposed to the highly cytotoxic **M3** remained a much lower number of viable cells.

At the end of the treatment, an interesting evolution of different stages was displayed by the cells treated with the studied materials. For example, in DLD-1 colon carcinoma the number of apoptotic cells was significantly higher for all types of treatment (one-way analysis of variance, Bonferroni post-test, $p<0.0001$) versus the untreated cells (Table 6, Figure 8). The metallodrug-functionalized materials, **M1**–**M3**, induced a significantly higher number of apoptotic cells when compared to the non-functionalized SBA-PADOH. Within 24 hours of treatment with the sub-cytotoxic doses, a small proportion of cells were already dead, except when using the material **M3** where the shift towards late apoptosis and cell death was accelerated.

In A2780 cells the same concentrations induced higher proportions of apoptotic cells, in both early and late stages, and the differences between functionalized and non-functionalized SBA-PADOH were also statistically significant. The cell loss was at a comparable level in all the metallodrug-functionalized materials, **M1**–**M3**, while SBA-PADOH induced an insignificant proportion of dead cells when compared with the untreated reference (one-way analysis of variance, $p<0.0001$).

Finally, the epidermal A431 cells were driven into apoptosis by all the studied materials (Table 6). The functionalization of SBA-PADOH with the metallodrugs benefits the evolution towards late apoptotic stages and cell death. In addition, the functionalization with metallodrugs did not dramatically increase the proportion of the cells blocked in early apoptotic stages. Furthermore, treatment with **M3** constrained the evolution towards strongly damaged and non-viable cells, in contrast with SBA-PADOH, where these populations were almost inexistent.

Biological Studies. Modulation of apoptotic signalling pathways by metallodrug-functionalized materials

In order to shed light on the possible mechanism of programmed cell death induced by the materials, we have looked into the tumour necrosis factor signalling as we have previously observed the influence of titanocene-functionalized SBA-15 materials on this factor.[33]

The TNF-α and the Fas receptor are two important players in the extrinsic apoptotic pathway. Therefore, their secretion was evaluated in tumour cells exposed to SBA-PADOH $SnPh_2Cl_2$, $TiCp_2Cl_2$, $TiCpCp^{PhNf}Cl_2$ and the materials **M1**–**M3**. The soluble Fas decreased significantly in all cell lines treated with the materials (Figure 9), however, an exception was found for **M3** which caused no changes in A431 cells (one-way analysis of variance, Bonferroni post-test, $p<0.0001$). The active organotin and titanocene precursors $SnPh_2Cl_2$, $TiCp_2Cl_2$, $TiCpCp^{PhNf}Cl_2$ do not exhibit any statistically significant influence on Fas receptor (one-way analysis of variances, $p<0.05$) (Figure S24 of supplementary material).

However, the FasLigand (FasL) production increased significantly in DLD-1 colon cells (Figure 10) after treatment with **M1** or **M2** (p value 0.0011). In A2780 ovary and A431 epidermoid carcinomas, only **M1** increased the FasL level (p value 0.0005 and 0.0229, respectively). On the other hand, the activity of the organotin and titanocene precursors $SnPh_2Cl_2$, $TiCp_2Cl_2$, $TiCpCp^{PhNf}Cl_2$ was irrelevant (Figure S25 of supplementary material).

The TNF-α secretion in the treated cells has a tendency to increase after cell contact with the metallodrug-functionalized materials **M1**–**M3** (Figure 11). However, the one-way analysis of variance indicates a significant increase only for **M2** and **M3** in DLD-1 colon (p value 0.0008) and A431 epidermoid carcinoma (p value 0.0016). The increase in TNF-α concentration in A2780 ovarian cells was not statistically significant in the 95% confidence interval. In this context, among the active precursors, only $SnPh_2Cl_2$ had demonstrated the capacity to modulate significantly the TNF-α level in the carcinoma cells (Figure S26 of supplementary material).

In this context, we have observed that SBA-PADOH did not exert any influence on Fas-FasL or TNF-α signalling pathways and the number of apoptotic cells increased after the prolonged contact with the tumour cells only in A2780 cell line, but the shift towards cell death was much slower. Almost all non-viable cells were found in early apoptotic stage, which denotes that the apoptotic process begun later, as in the functionalized materials, and only in 2% of the

population cell death did occur within 24 hours. This is in clear contrast with the metallodrug-functionalized materials **M1**–**M3** where the percentage of dead cells was between ca. 16–20%.

It is well known in the literature that organotin compounds are able to induce apoptosis in tumour cells, including colon,[51] ovary[12] and skin cell lines.[52] The treatment with the organotin-functionalized material (**M1**) triggered extrinsic apoptosis by influencing the Fas-FasL pathway with the biological target being the FasLigand and not the membranar Fas itself (Figures 9-11). This type of behaviour has previously been described in reports on non-supported organotin compounds[53] and titanocenes derivatives,[54] which were able to trigger apoptosis by the modulation of Fas levels in tumour cells. However, the results presented here are, to the best of our knowledge, the first in which the modulation of Fas levels in metallodrug-functionalized nanostructured silica-based materials is confirmed.

In contrast, it is has been reported that certain metallocene complexes of vanadium and molybdenum are able to trigger extrinsic apoptosis[55] and that the TNF pathway can be modulated by titanocene-functionalized materials through the TNFR1 receptor.[33] In this study we have confirmed that titanocene-functionalized SBA-15 systems such as **M2** and **M3** are able to trigger apoptosis by interfering with the TNF-α pathway and not through Fas-FasL system, which appears to be unaffected. Bearing in mind that TNF-α has the ability to induce protein kinase mediated apoptosis in colorectal cancer by redirecting pro-survival heat-shock transcription factors to the apoptotic pathway,[56] and that TNF-α triggers apoptosis[57] via SH3KBP1-binding protein1 in ovarian cancer and stimulates the inhibition of the proapoptotic proteins in A431 epidermal carcinoma cells,[58] our results suggest that the mechanism of action of titanocene-functionalized silica-based materials undergo similar pathways, which are very different to those described in the literature for non-supported titanocene derivatives and other metallodrugs.

Conclusions

SBA-15 has been functionalized with an aminodiol ligand PADOH and subsequently reacted with tin or titanium metallodrugs to give three different metallodrug-functionalized SBA-15-based materials which have been synthesized and characterized by different techniques. While the SBA-PADOH material did not show any significant cytotoxic activity, the metallodrug-functionalized materials showed a moderate antiproliferative activity, showing that the role of the PADOH ligand is limited to facilitating the support of the tin- or titanium-containing moieties, which are the responsible of the cytotoxic action of the reported systems. In addition, our study has demonstrated that the proapoptotic capacity of the metallodrug-functionalized materials rely on their functionalization with active prodrugs such as organotin or titanocene derivatives. Thus, a simple change in the design of the nanostructured material by including a different metallodrug will have influence on the metabolic activity of the tumour cells, modulating the apoptotic pathways by different mechanisms, according to the active compound inside the material. It has also been demonstrated that the titanocene-functionalized SBA-15 materials are able to trigger apoptosis by interfering with the TNF-α pathway while the tin-functionalized SBA-15 materials induce apoptosis through the Fas-FasL system.

In summary, we have demonstrated that the incorporation of different metallodrugs of different metal ions leads to different mechanisms of apoptosis induction, confirming that acting as a whole particle and with the help of the release of a very small quantity of metallodrug (10% of Sn in **M1** and less than 1% of Ti in **M2** and **M3**), the design of the supported metal complex and

its functionalization have a crucial influence on their anticancer mechanism of action against a wide variety of cancer cell lines.

Acknowledgments

We gratefully acknowledge financial support from the Ministerio de Economía y Competitividad Spain – FEDER (Grant nos. CTQ2015-66164-R and CTQ2017-90802-REDT) and the Romanian UEFISCDI Grant PN-III-P2-2.1-PED-2016-1857. We would also like to thank Universidad Rey Juan Carlos and Banco de Santander for supporting our Research Group of Excellence QUINANOAP. Finally, we thank for valuable advice C. Rodríguez, S. Carralero and C. Forcé.

Figures, Schemes and Tables

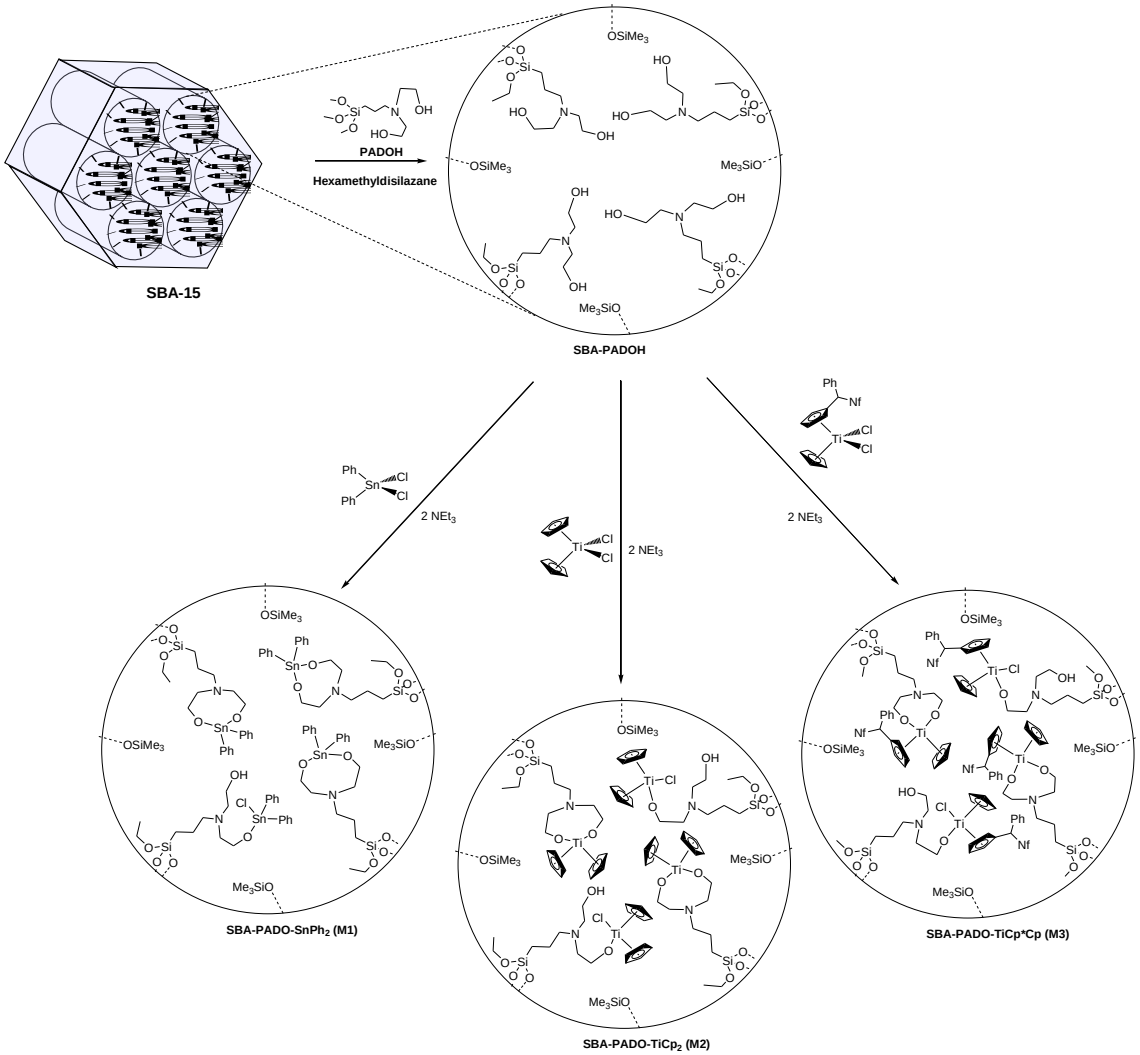

Scheme 1. Synthesis of metallodrug-functionalized materials

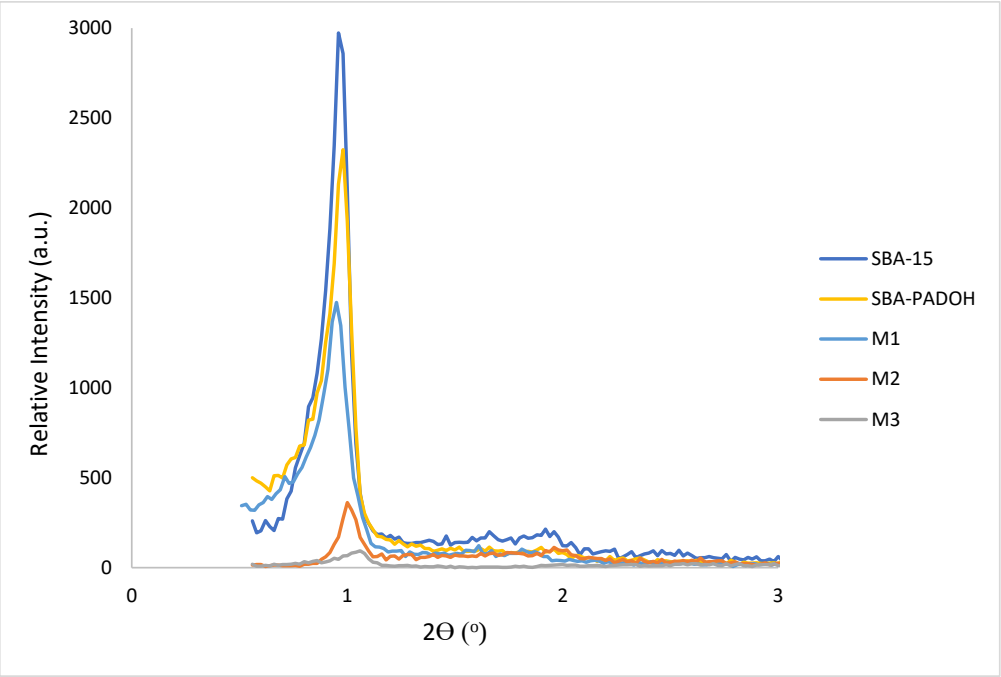

Figure 1. XRD diffraction patterns of SBA-15, SBA-PADOH and **M1**–**M3**

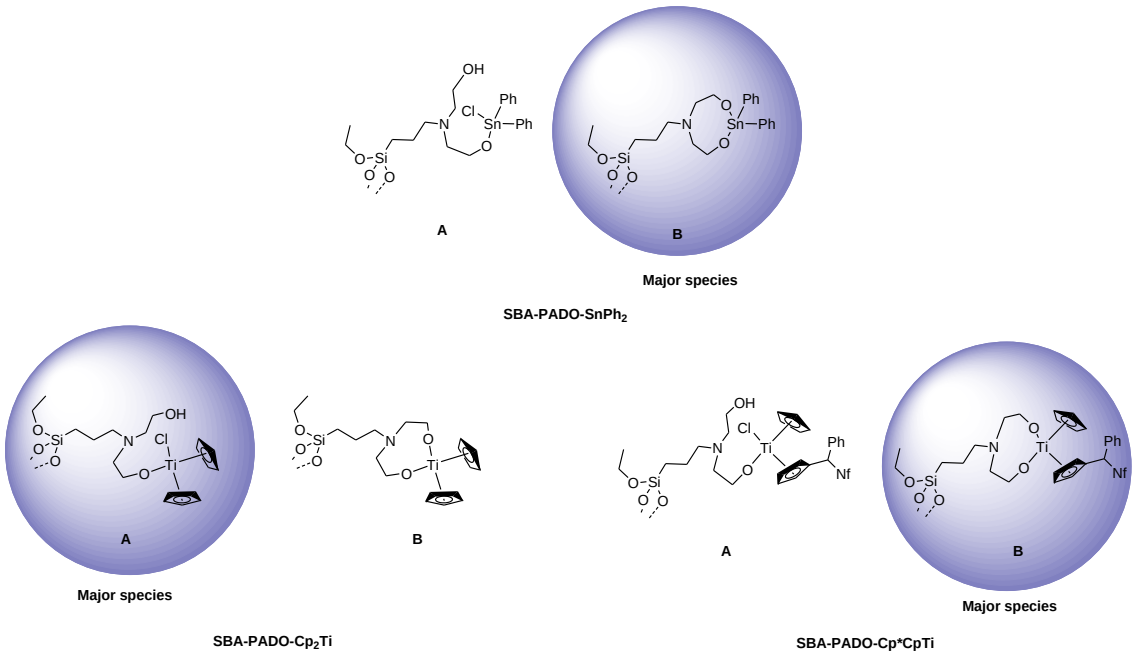

Figure 2. Functionalization species: A) product of the reaction with one M-Cl bond; B) product of the reaction with both M-Cl bonds. Major species for each material are highlighted

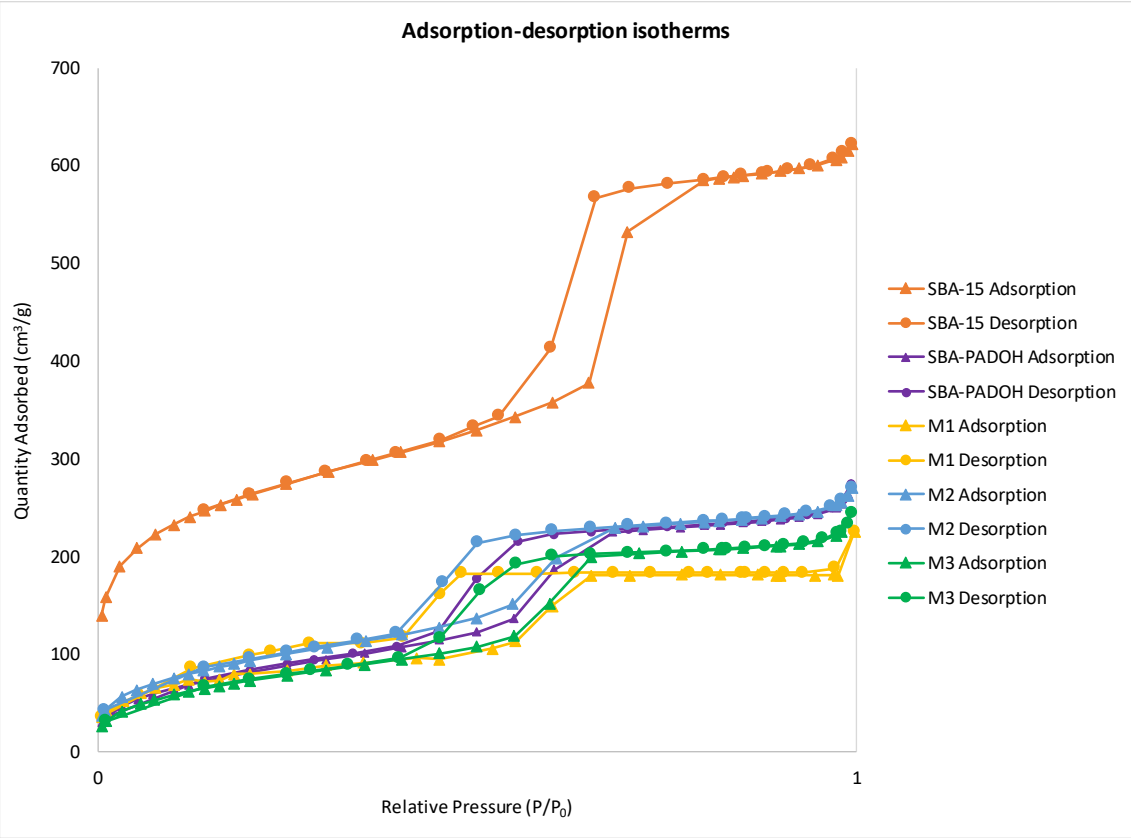

Figure 3. Nitrogen adsorption/desorption isotherms of SBA-15, SBA-PADOH and **M1**–**M3**

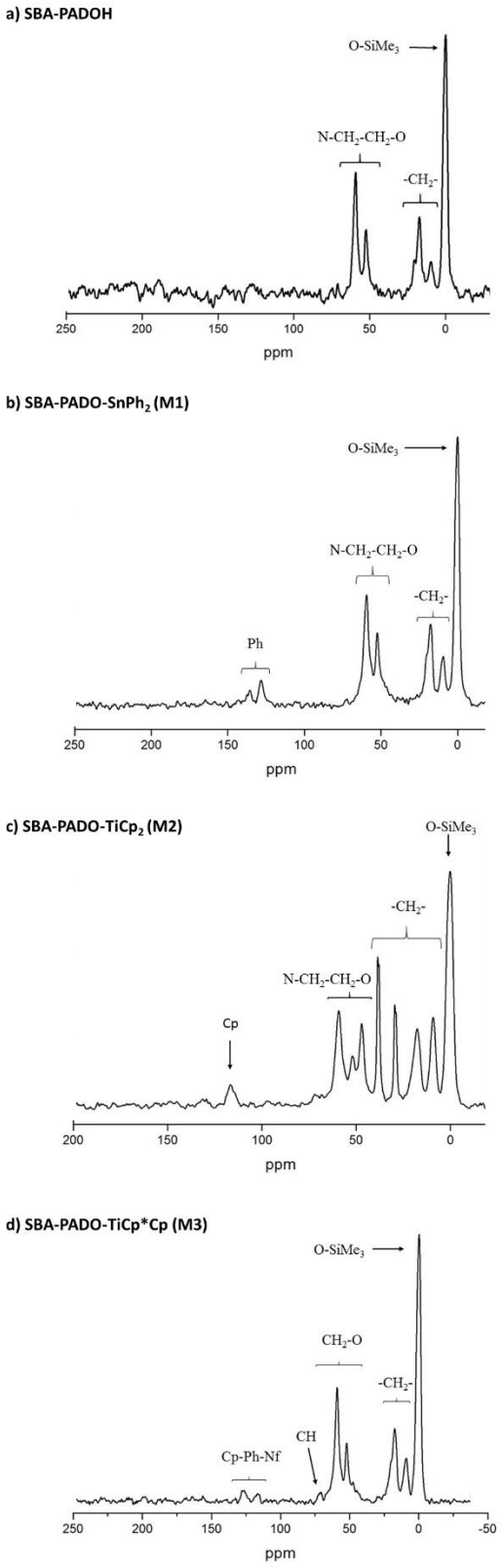

Figure 4. ^{13}C CP MAS spectra of SBA-PADOH and **M1**–**M3**

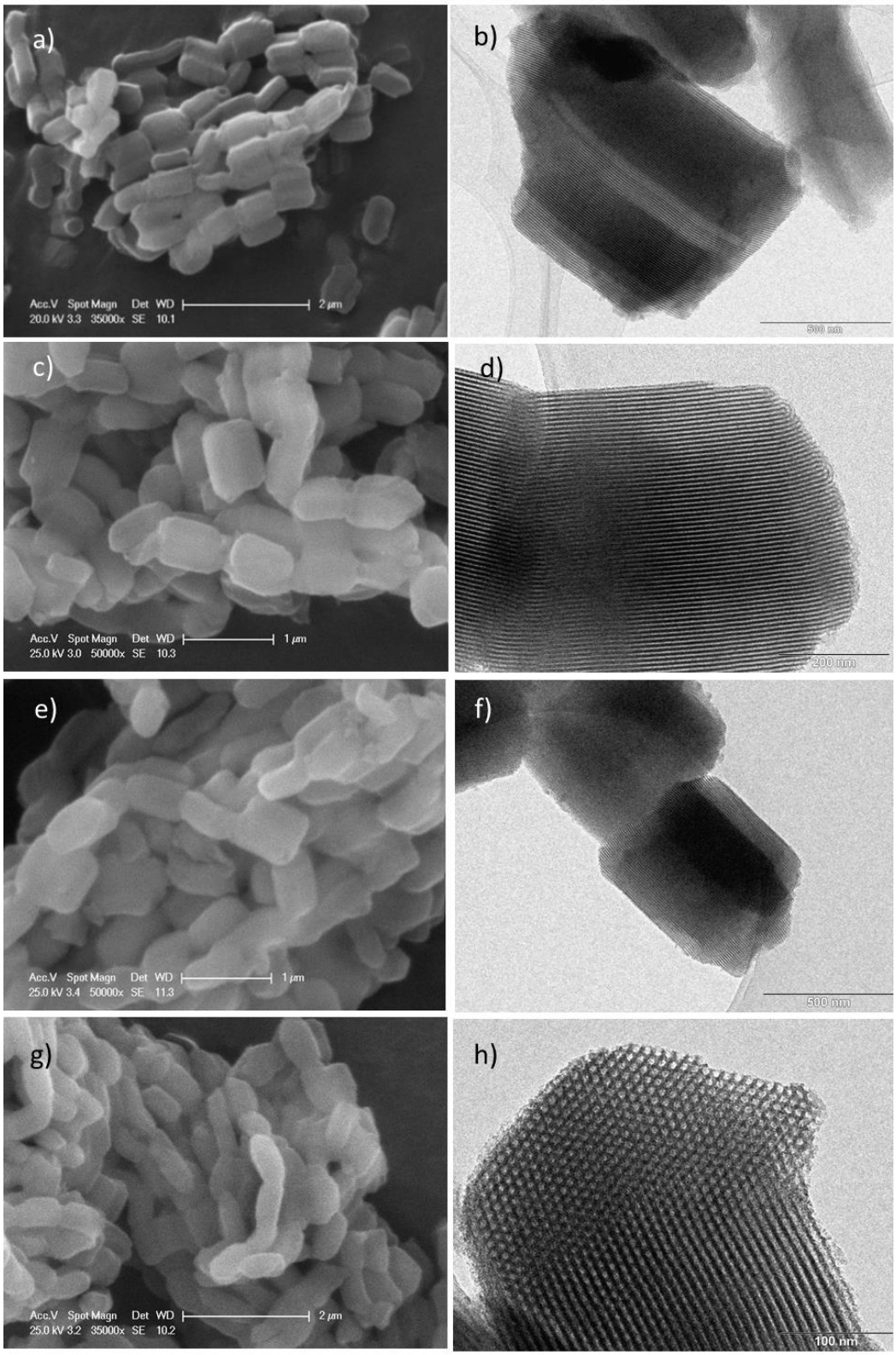

Figure 5. SEM images of SBA-PADOH (a), **M1** (c), **M2** (e) and **M3** (g) and TEM images of SBA-PADOH (b), **M1** (d), **M2** (f) and **M3** (h)

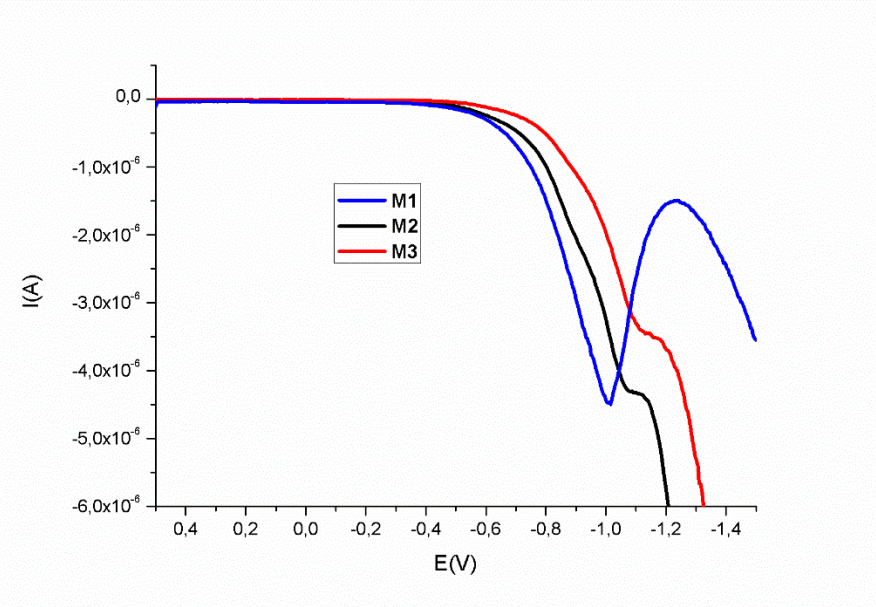

Figure 6. Differential pulse voltammograms (75 mV modulation amplitude) of **M1**–**M3**/graphite electrode immediately after immersion in aqueous phosphate buffer pH 7.4 vs Ag/AgCl/KCl (3 M) as reference electrode

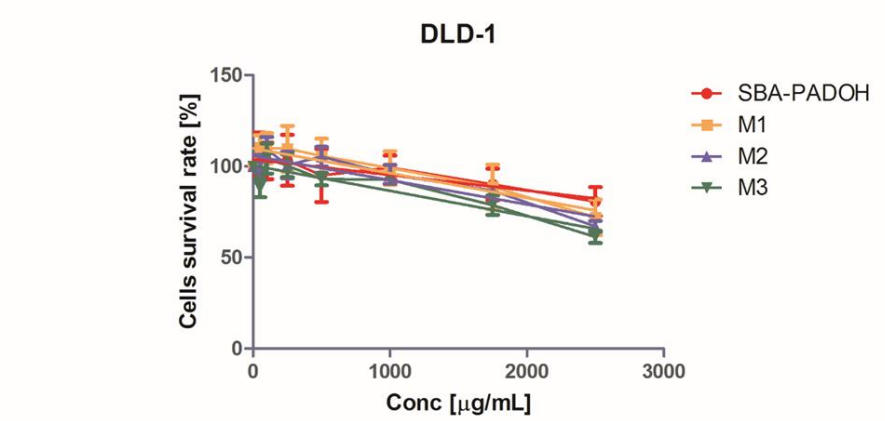

	SBA-PADOH	M1	M2	M3
Slope	-0.00857 ± 0.00364	-0.0136 ± 0.00343	-0.0133 ± 0.00219	-0.0139 ± 0.00217

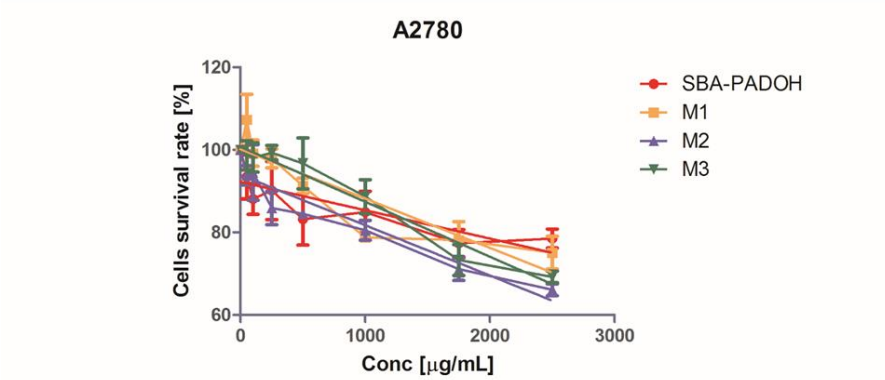

	SBA-PADOH	M1	M2	M3
Slope	-0.006869 ± 0.001902	-0.01196 ± 0.001682	-0.01218 ± 0.001392	-0.01331 ± 0.001338

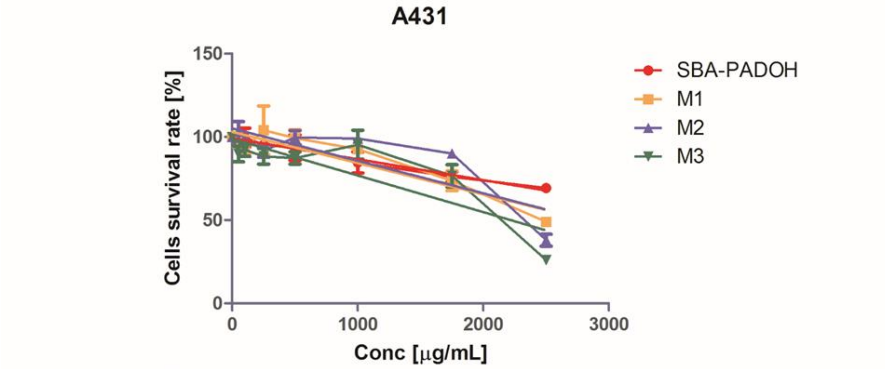

	SBA-PADOH	M1	M2	M3
Slope	-0.01255 ± 0.001582	-0.01880 ± 0.002628	-0.01948 ± 0.003022	-0.02201 ± 0.003313

Figure 7. Metabolic activity reduction in treated cancer cells. The negative Hill slope indicates that the metabolic activity drop in dose-dependent manner after the cells exposure to the studied materials SBA-PADOH and **M1**–**M3**

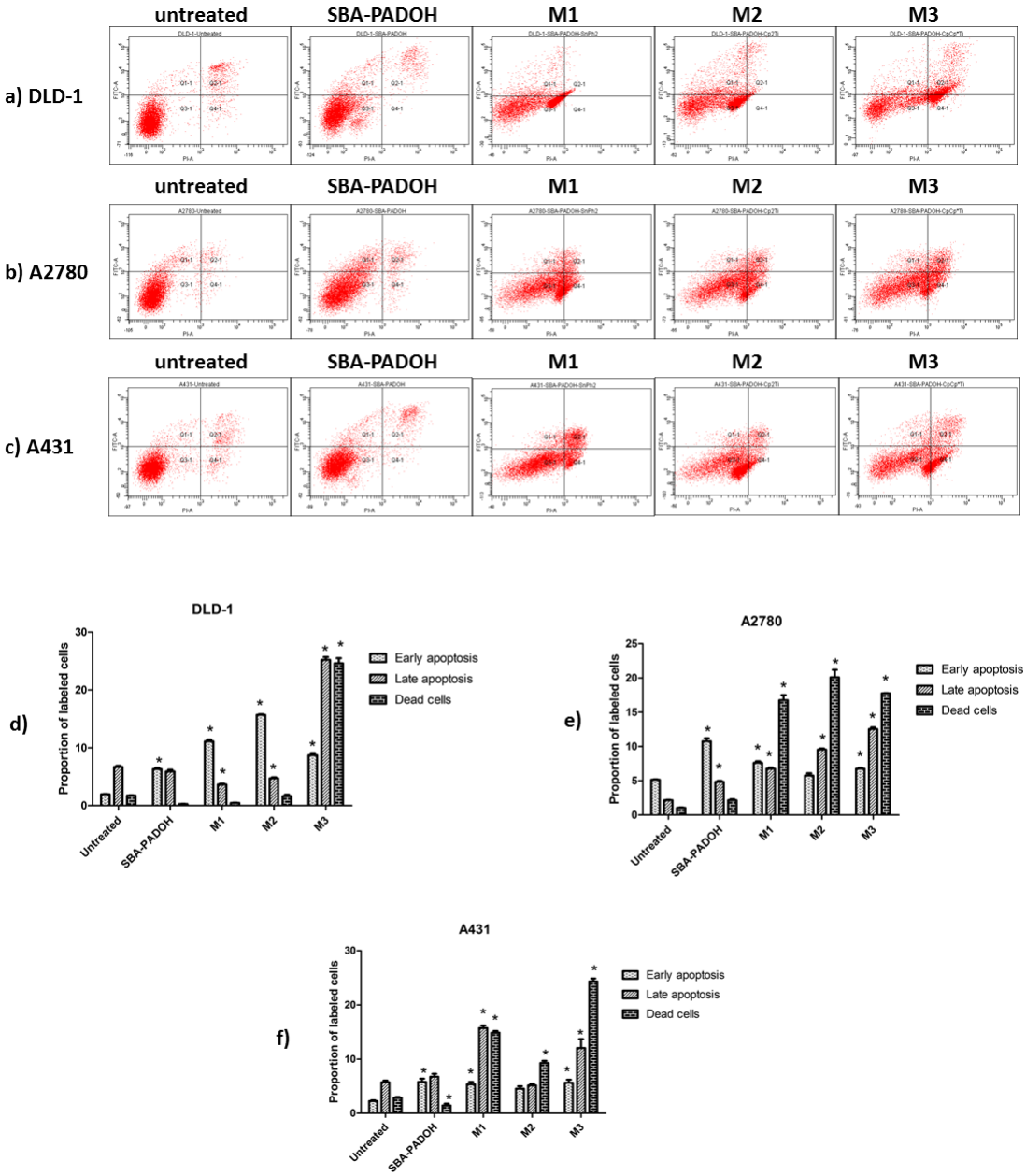

Figure 8. Apoptosis induction in tumour cells (a) DLD-1, (b) A2780 and (c) A431 treated with SBA-PADOH and **M1**–**M3**. In the histograms obtained by flow cytometry, the left lower quartile (Q3) contains the unstained, living cells, the right lower quartile (Q4) the PI-labelled dead cells, the upper left quartile the apoptotic cells which displays fluorescence at 488 nm (Alexa Fluor 488 stain) and the upper right quartile the double coloured, late apoptotic cells. (d-f) Distribution of the early apoptotic, late apoptotic and necrotic cells within a population of 10000 cells after treatment; the starred columns represent the significant different proportion *vs.* the untreated control populations.

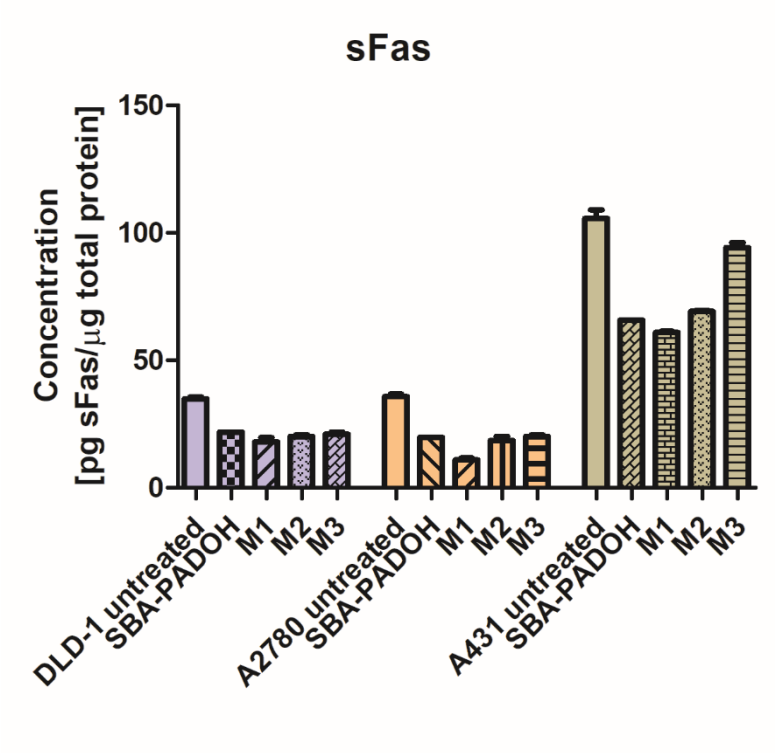

Figure 9. Concentrations (pg/μg total protein) of soluble Fas apoptosis signal receptor secreted by tumour cells treated *in vitro* with SBA-PADOH and **M1**–**M3**

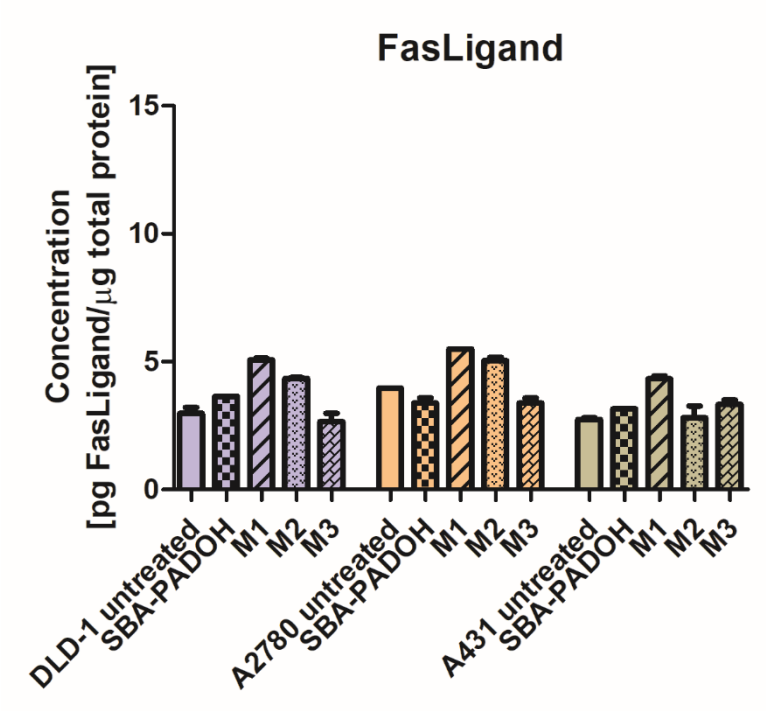

Figure 10. Modulation of soluble FasLigand in cells treated with SBA-PADOH and **M1**–**M3**

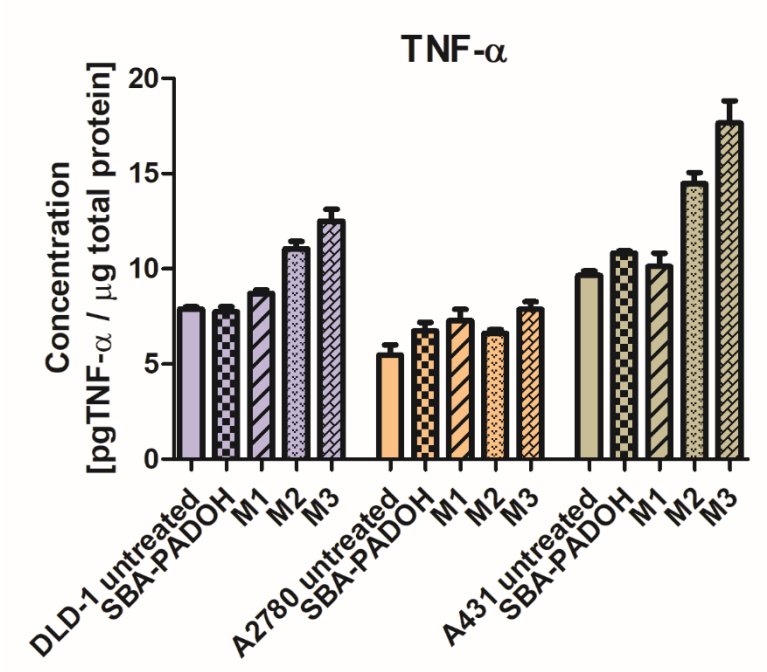

Figure 11. Tumour necrosis factor alpha concentrations (pg/ μg total protein) in colon, ovarian and epidermoid carcinoma cell populations following the 24-hour treatment with sub-cytotoxic concentrations of SBA-PADOH and **M1**–**M3**

Table 1. XRD data of the synthesized materials SBA-15, SBA-PADOH and **M1**–**M3**

Material	$(\boldsymbol{hkl})$	**2Θ(˚)**	$\boldsymbol{d_{hkl}}(\text{Å})$	$\mathbf{a_o}(\text{Å})$
SBA-15	100	0.95	93.03	107.2
	110	1.89		
SBA-PADOH	100	0.96	92.05	106.3
	110	1.85		
SBA-PADO-$SnPh_2$ (**M1**)	100	0.97	91.24	105.4
	110	1.98		
SBA-PADO-$TiCp_2$ (**M2**)	100	1.01	87.59	101.1
	110	1.97		
SBA-PADO-TiCp*Cp (**M3**)	100	1.04	84.74	97.9
	110	1.98		

Table 2. Percentage of tin, titanium or chlorine grafted on the silica support

Material	Theoretical Sn % wt.	Theoretical Ti % wt.	Experimental Ti % wt.	Experimental Sn % wt.	Experimental Cl % wt.	Experimental Molar ratio Sn:Cl or Ti:Cl
M1	15.0	-	-	12.4	1.0	3.8:1
M2	-	5.0	3.2	-	2.2	1.1:1
M3	-	5.0	2.0	-	0.8	1.8:1

Table 3. Physical parameters of SBA-15, SBA-PADOH and **M1**–**M3** measured by N_2 adsorption-desorption isotherms

Material	BET Surface (m^2/g)	Pore Volume (cm^3/g)	Pore Size (nm)
SBA-15	931	0.85	5.37
SBA-PADOH	306	0.39	3.64
M1	286	0.28	3.52
M2	347	0.39	3.32
M3	275	0.34	3.62

Table 4. Release studies of materials **M1**–**M3** in simulated body fluid

t (h)	M1		M2		M3	
	Sn (ppm) in solution	% of release of loaded Sn	Ti (ppm) in solution	% of release of loaded Ti	Ti % wt in solution	% of release of loaded Ti
0	0	0	0	0	0	0
1	4.11	2.21	0.14	0.29	0.14	0.30
6	10.40	5.60	0.15	0.33	0.16	0.36
24	18.79	10.10	0.16	0.34	0.17	0.37
48	19.80	10.64	0.19	0.41	0.19	0.39
96	19.57	10.52	0.20	0.42	0.37	0.78

Table 5. Cell growth inhibitory effect of SBA-PADOH, metal precursors and functionalized materials **M1**–**M3** against colon (DLD-1), ovarian (A2780) and epidermal (A431) carcinoma *in vitro*, expressed as half maximal effective values.

Cell type	**Best-fit EC_{50} values (p<0.05) [µg/mL] of materials**	**SBA-PADOH**	**M1**	**M2**	**M3**
DLD-1	**EC_{50}**	**515.9**	**224.3**	**207.4**	**167.7**
	$logEC_{50}$ ± SD	2.71± 0.09	2.35 ± 0.15	2.32 ± 0.09	2.23 ± 0.10
A2780	**EC_{50}**	**777.4**	**572.4**	**365.5**	**299.2**
	$logEC_{50}$ ± SD	2.89 ± 0.07	2.76 ± 0.08	2.56 ± 0.07	2.48 ± 0.09
A431	**EC_{50}**	**651.4**	**472.5**	**505.4**	**325.8**
	$logEC_{50}$ ± SD	2.81 ± 0.04	2.67 ± 0.05	2.70 ± 0.06	2.51 ± 0.05
	Best-fit EC_{50} values (p<0.05) [µg/mL] of precursors		**$SnPh_2Cl_2$**	**Cp_2TiCl_2**	**$CpCp^{PhNf}TiCl_2$**
DLD-1	**EC_{50}**		250.6	456.9	317.7
	$logEC_{50}$ ± SD		2.40±0.13	2.66±0.11	2.50±0.23
A2780	**EC_{50}**		565.7	421.2	363.7
	$logEC_{50}$ ± SD		2.75±0.18	2.63±0.09	2.56±0.11
A431	**EC_{50}**		557.3	611.8	463.7
	$logEC_{50}$ ± SD		2.75±0.15	2.79±0.20	2.67±0.18

Table 6. Proportion (%) of apoptotic cells in tumour cell populations (DLD-1, A2780 and A431) treated with SBA-PADOH and **M1**–**M3** materials

Cell type	Treatment	Early apoptosis	Late apoptosis	Dead cells	Living cells
DLD-1	Untreated	2.0±0.1	6.9±0.3	1.8±0.1	89.2±0.5
	SBA-PADOH	6.3±0.3	5.8±0.4	0.2±0.1	87.7±0.5
	M1	11.2±0.5	3.6±0.2	0.4±0.1	84.8±0.1
	M2	15.7±0.2	4.7±0.3	1.6±0.4	78.0±0.5
	M3	8.3±0.6	25.2±0.7	25.5±1.3	40.9±0.5
A2780	Untreated	5.1±0.1	2.1±0.1	1.0±0.1	91.8±2.0
	SBA-PADOH	10.7±0.7	4.9±0.2	2.0±0.3	82.4±0.2
	M1	7.4±0.3	6.6±0.2	16.3±1.1	69.7±0.7
	M2	5.7±0.5	9.5±0.2	20.0±1.1	64.8±1.3
	M3	6.7±0.2	12.7±0.4	17.7±0.8	62.9±0.3
A431	Untreated	2.4±0.2	5.4±0.5	3.0±0.3	89.2±0.9
	SBA-PADOH	5.2±0.9	7.3±0.7	0.9±0.5	86.6±1.1
	M1	4.9±0.7	16.2±0.7	15.2±0.5	63.7±0.4
	M2	4.1±0.4	5.4±0.4	9.7±0.6	80.8±2.3
	M3	5.1±0.8	10.4±1.1	23.8±0.8	60.7±0.8

References

1 B. Rosenberg, L. V. Camp, *Canc. Res.* 1970, **30**, 1799–1802.
2 K. D. Mjos, C. Orvig, *Chem. Rev.* 2014, **114**, 4540–4563.
3 U. Ndagi, N. Mhlongo, M. E. Soliman, *Drug Des Devel Ther.* 2017, **11**, 599–616.
4 N. Metzler-Nolte, Z. Guo (Ed.) Themed Issue in Dalton Transactions: Metallodrugs: Activation, Targeting, and Delivery, *Dalton Trans.*, 2016, **45**, 12965–13069
5 P. Zhang, P. J. Sadler, *J. Organomet. Chem.* 2017, **839**, 5–14.
6 A. Korfel, M. E. Scheulen, H. J. Schmoll, O. Gründel, A. Harstrick, M. Knoche, L. M. Fels, M. Skorzec, F. Bach, J. Baumgart, G. Sass, S. Seeber, E. Thiel, W. E. Berdel, *Clin. Cancer Res.* 1998, **4**, 2701–2708.
7 N. Kröger, U. R. Kleeberg, K. Mross, L. Edler, D. K. Hossfeld, *Onkologie* 2000, **23**, 60–62.
8 H. Skoupilova, R. Hrstka, M. Bartosik, *Med. Chem.* 2017, **13**, 334–344.
9 U. Olszewski, G. Hamilton, *Anticancer Agents Med. Chem.* 2010, **10**, 302–311.
10 K Strohfeldt, M Tacke, *Chem. Soc. Rev.* 2008, **37**, 1174–1187.
11 Y. Ellahioui, S. Prashar, S. Gómez-Ruiz, *Inorganics* 2017, **5**, 4.
12 G. N. Kaluđerović, H. Kommera, E. Hey-Hawkins, R. Paschke, S. Gómez-Ruiz, *Metallomics* 2010, **2**, 419–428.
13 L. Rocamora-Reverte, E. Carrasco-García, J. Ceballos-Torres, S. Prashar, G. N. Kaluđerović, J. A. Ferragut, S. Gómez-Ruiz, *ChemMedChem* 2012, **2**, 301–310.
14 L. Astolfi, S. Ghiselli, V. Guaran, M. Chicca, E. Simoni, E. Olivetto, G. Lelli, A. Martini, *Oncol Rep.* 2013, **29**, 1285–1292.
15 W. Wani, S. Prashar, S. Shreaz, S. Gómez-Ruiz, *Coord. Chem. Rev.* 2016, **312**, 67–98.
16 Y. Ellahioui, S. Prashar, S. Gómez-Ruiz, *Curr. Med. Chem.* 2016, **23**, 4450–4467.
17 J. Wang, Q. Chen, N. Tian, W. Zhu, H. Zou, X. Wang, X. Li, X. Fan, G. Jiang and B. Z. Tang, *J. Mater. Chem. B,* 2018, **6**, 1595–1599.
18 A. Boulmier, X. Feng, O. Oms, P. Mialane, E. Rivière, C. J. Shin, J. Yao, T. Kubo, T. Furuta, E. Oldfield and A. Dolbecq, *Inorg. Chem.* 2017, **56**, 7558–7565.
19 L. Wang, K. Yu, J. Zhu, B. B. Zhou, J. R. Liu and G. Y. Yang, *Dalton Trans.*, 2017, **46**, 2874–2883.
20 Z.-M. Zhang, X. Duan, S. Yao, Z. Wang, Z. Lin, Y.-G. Li, L.-S. Long, E.-B. Wang and W. Lin, *Chem. Sci.,* 2016, **7**, 4220–4229.
21 S. She, S. Bian, R. Huo, K. Chen, Z. Huang, J. Zhang, J. Hao and Y. Wei, *Sci. Rep.* 2016, **6**, 33529.
22 A. Saad, W. Zhu, G. Rousseau, P. Mialane, J. Marrot, M. Haouas, F. Taulelle, R. Dessapt, H. Serier-Brault, E. Rivière, T. Kubo, E. Oldfield and A. Dolbecq, *Chem. Eur. J.* 2015, **21**, 10537–10547.
23 S. She, S. Bian, J. Hao, J. Zhang, J. Zhang and Y. Wei, *Chem. Eur. J.* 2014, **20**, 16987–16994.
24 L. Wang,K. Yu, B.-B. Zhou, Z.-H. Su, S. Gao, L.-L. Chua and J.-R. Liu, *Dalton Trans.*, 2014, **43**, 6070–6078.
25 L. Wang, B.-B. Zhou, K. Yu, Z.-H. Su, S. Gao, L.-L. Chua, J.-R. Liu and G.-Y. Yang, *Inorg. Chem.* 2013, **52**, 5119–5127.
26 Y. Zhang, R. Cao, F. Yin, M. P. Hudock, R.-T. Guo, K. Krysiak, S. Mukherjee, Y.-G. Gao, H. Robinson, Y. Song, J. H. No, K. Bergan, A. Leon, L. Cass, A. Goddard, T.-K. Chang, F.-Y. Lin, E. Van Beek, S. Papapoulos, A. H.-J. Wang, T. Kubo, M. Ochi, D. Mukkamala and E. Oldfield, *J. Am. Chem. Soc.,* 2009, **131**, 5153–5162.
27 D. Pérez-Quintanilla, S. Gómez-Ruiz, Z. Žižak, I. Sierra, S. Prashar, I. Del Hierro, M. Fajardo, Z. D. Juranić, G. N. Kaluđerović, *Chem. Eur. J.* 2009, **15**, 5588–5597.
28 G. N. Kaluđerović, D. Pérez-Quintanilla, I. Sierra, S. Prashar, I. Del Hierro, Z. Žižak, Z. D. Juranić, M. Fajardo, S. Gómez-Ruiz, *J. Mater. Chem.* 2010, **20**, 806–814.
29 G. N. Kaluđerović, D. Pérez-Quintanilla, Z. Žižak, Z. D. Juranić, S. Gómez-Ruiz, *Dalton. Trans.* 2010, **39**, 2597–2608.
30 A. García-Peñas, S. Gómez-Ruiz, D. Pérez-Quintanilla, R. Paschke, I. Sierra, S. Prashar, I. Del Hierro, G. N. Kaluđerović, *J. Inorg. Biochem.* 2012, **116**, 100–110.
31 J. Ceballos-Torres, P. Virag, M. Cenariu, S. Prashar, M. Fajardo, E. Fischer-Fodor, S. Gómez-Ruiz, *Chem. Eur. J.* 2014, **20**, 10811–10828.
32 J. Ceballos-Torres, S. Prashar, M. Fajardo, A. Chicca, J. Gertsch, A. B. Pinar, S. Gómez-Ruiz, *Organometallics* 2015, **34**, 2522–2532.
33 S. Gómez-Ruiz, A. García-Peñas, S. Prashar, A. Rodríguez-Diéguez, E. Fischer-Fodor, *Materials* 2018, **11**, 224.

34 M. Z. Bulatović, D. Maksimović-Ivanić, C. Bensing, S. Gómez-Ruiz, D. Steinborn, H. Schmidt, M. Mojić, A. Korać, I. Golić, D. Pérez-Quintanilla, M. Momčilović, S. Mijatović, G. N. Kaluđerović, *Angew. Chem. Int. Ed.* 2014, **53**, 5982–5987.
35 C. Bensing, M. Mojić, S. Gómez-Ruiz, S. Carralero, D. Maksimović-Ivanić, S. Mijatović, G. N. Kaluđerović, *Dalton Trans.* 2016, **45**, 18984–18993.
36 M. Cini, T. N. Bradshaw, S. Woodward, *Chem. Soc. Rev.* 2017, **46**, 1040–1051.
37 L. Yeruva, J. A. Elegbede, S. W. Carpera, *Anticancer Drugs* 2008, **19**, 766–776.
38 L. C. Fairclough, A. A. Stoop, O. H. Negm, P. M. Radford, P. J. Tighe, I. Todd, *Eur. J. Immunol.* 2015, **45**, 2937–2944.
39 H. M. Yun, K. R. Park, E. C. Kim, S. B. Han, D. Y. Yoon, J. T. Hong, *Oncotarget* 2015, **6**, 9061–9072.
40 H. Wang, J. Liu, X. Hu, S. Liu, B. He, *Med. Sci. Monit.* 2016, **22**, 3694–3704.
41 J. Ceballos-Torres, S. Gómez-Ruiz, G. N. Kaluderovic, M. Fajardo, R. Paschke, S. Prashar, *J. Organomet. Chem.* 2012, **700**, 188–193.
42 D. Zhao, Q. Huo, J. Feng, B. Chmelka, G. Stucky, *J. Am. Chem. Soc.* 1998, **120**, 6024–6036.
43 Y. Pérez, I. del Hierro, L. Zazo, R. Fernández-Galán, M. Fajardo, *Dalton Trans.* 2015, **44**, 4088–4101.
44 P. Horcajada, A. Rámila, J. Pérez-Pariente, M. Vallet-Regí, *Microp. Mesop. Mat.* 2004, **68**, 105–109.
45 N. Miklásová, E. Fischer-Fodor, P. Lönnecke, M. Perde Schrepler, P. Virag, C. Tatomir, V. I. Cernea, E. Hey-Hawkins, L. Silaghi-Dumitrescu, *J. Inorg. Biochem*. 2009, **103**, 1739–1747.
46 N. Miklášová, E. Fischer-Fodor, R. Mikláš, L. Kucková, J. Kožíšek, T. Liptaj, O. Soritau, J. Valentová, F. Devínsky, *Inorg. Chem. Commun.* 2014, **46**, 229–233.
47 K. S. W. Sing, D. H. Everett, R. A. W. Haul, L. Moscou, R. A. Pierotti, J. Rouquérol, T. Siemieniewska, *Pure Appl. Chem.* 1985, **57**, 603–620.
48 M. Thommes, K. Kaneko, A. V. Neimark, J. P. Olivier, F. Rodriguez-Reinoso, J. Rouquerol, K. S. W. Sing, *Pure Appl. Chem.* 2015, **87**, 1051–1069.
49 I. Hierro, Y. Pérez, M. Fajardo, *J. Solid. State. Electrochem.* 2015, **19**, 2063–2074.
50 I. Hierro, Y. Pérez, M. Fajardo, *Appl. Organometal. Chem.* 2016, **30**, 208–214.
51 A. Varela-Ramírez, M. Costanzo, Y. P. Carrasco, K. H. Pannell, R. J. Aguilera, *Cell Biol. Toxicol.* 2011, **27**, 159–168.
52 M. A. Costa, L. Gulino, L. Pellerito, T. Fiore, C. Pellerito, G. Barbieri, *Oncol. Rep.* 2009, **21**, 593–599.
53 C. P. Schröder, H. R. Maurer, *Cancer Immunol. Immunother*. 2001, **50**, 69–76.
54 L. Kater, J. Claffey, M. Hogan, P. Jesse, B. Kater, S. Strauss, M. Tacke, A. Prokop, *Toxicol. In Vitro* 2012, **26**, 119–124.
55 L. Sebestova, R. Havelek, M. Rezacova, J. Honzicek, Z. Krocova, J. Vinklarek, *Chem. Biol. Interact.* 2015, **242**, 61–70.
56 N. Benderska, J. Ivanovska, T. T. Rau, J. Schulze-Luehrmann, S. Mohan, S. Chakilam, M. Gandesiri, E. Ziesché, T. Fischer, S. Söder, A. Agaimy, L. Distel, H. Sticht, V. Mahadevan, R. Schneider-Stock, *J. Cell. Sci.* 2014, **127**, 5273–5287.
57 J. P Liu, N. S. Liu, H. Y. Yuan, Q. Guo, H. Lu, Y. Y. Li, *Mol. Cell Biochem*. 2006, **292**, 189–195.
58 A. Faurschou, R. Gniadecki, D. Calay, H. C. Wulf, *J. Invest. Dermatol*. 2008, **128**, 2069–2077.